

Development of a triple impinging jet mixer for continuous antisolvent crystallization of acetylsalicylic acid reaction mixture

Kornélia Tacsí^a, Ádám Joó^a, Éva Pusztai^b, András Domokos^a, Zsombor K. Nagy^a, György Marosi^{a,*}, Hajnalka Pataki^a

^a Budapest University of Technology and Economics, Department of Organic Chemistry and Technology, Műegyetem rkp. 3, Budapest 1111, Hungary

^b Budapest University of Technology and Economics, Department of Chemical and Environmental Process Engineering, Műegyetem rkp. 3, Budapest 1111, Hungary

ARTICLE INFO

Keywords:

Continuous crystallization
Impinging jet
Overflow
MSMPR
Acetylsalicylic acid
Reaction mixture
Design of experiments

ABSTRACT

This study aims to develop a continuous antisolvent crystallization technique using a novel non-submerged triple impinging jet mixer for multiple feeding volume ratios to perform the direct procession of a flow acetylsalicylic acid (ASA) reaction mixture. The impinging jet mixer was supplemented by an overflow mixed suspension mixed product removal (MSMPR) crystallizer to provide a longer aging period for the crystals. The effect of temperature, residence time, and antisolvent to ASA solution ratio on product purity, yield, productivity, crystal size, and crystal size distribution was examined applying a 2³ two-level full factorial experimental design. It was found that due to the intensive initial mixing achieved with triple impinging jet significantly smaller crystal size (<180 μm) with narrower unimodal crystal size distribution and higher maximum yield (83.1%) could be obtained compared to the conventional MSMPR technique. Furthermore, the developed continuous crystallization was accomplished in smaller equipment with the same productivity. Consequently, the processing of the ASA reaction mixture using a triple impinging jet mixer system enables the morphology modification and the direct connection of flow synthesis with continuous crystallization step.

1. Introduction

Rapid, homogeneous, and efficient mixing is essential for continuous crystallization especially in the case of fast crystallization processes with high supersaturation, such as antisolvent and reactive crystallizations where highly miscible fluid components have to be agitated. Mixing ensures homogeneous supersaturation and nucleation resulting in narrow crystal size distribution (CSD) [1,2]. Accordingly, the techniques of mixing are intensely studied in the literature, therefore many solutions are described in publications such as traditional T- [3], Y-mixers [4], special Roughton type vortex mixers [5], radial mixers [6–8], static mixers [9,10], ultrasound irradiation [11], and impinging jet (IJ) techniques [12].

Among these, the IJ mixers rapidly impinge two liquid streams at a very high velocity (1.0–15.0 m/s) to produce a homogeneous system without external mechanical mixing [13]. In many publications, this technique is called a dual impinging jet (DIJ) [13], or a two-impinging-jet mixer (TIJ) [14]. Normally jets with similar volumetric flow rates are mixed, but this method can be also used for mixing

streams up to a 2:1 volumetric ratio. If jets with a greater feeding volume ratio are applied, it can cause inappropriate mixing profiles and splattering. Liu et al. [15] tested the collision of parallel fluid jets at a 4:1 volume ratio. They reported the shift of the stream meeting point to the jet outlet of fluid with a lesser amount of feed and a smaller diameter, which caused gradually the product accumulation on this tube outlet and its clogging. To avoid direct frontal collision and thereby clogging issues 10° downward jets were used. Zhang et al. tested a free triple impinging jet mixer with two horizontal opposite and a perpendicular jet configuration to study the turbulent behavior of mixing by unequal liquid streams in a liquid-liquid reaction [16].

In some studies, IJ mixers were used for submicronic particle precipitation and production. Thus, the IJ technique gains increased importance in the case of poorly water-soluble drugs [17], as crystal size reduction enhances the dissolution rate of these drugs increasing their bioavailability [18]. As defined above, the IJ mixer can also be used for the in situ seedings of continuous crystallizers in order to reduce the crystal size and producing narrow CSD [19,20]. Advantageously, higher productivity can be reached comparing to top-down (milling,

* Corresponding author.

E-mail addresses: marosi.gyorgy@vbk.bme.hu (G. Marosi), pataki.hajnalka@vbk.bme.hu (H. Pataki).

<https://doi.org/10.1016/j.cep.2021.108446>

Received 10 December 2020; Received in revised form 21 April 2021; Accepted 23 April 2021

Available online 1 May 2021

0255-2701/© 2021 The Authors. Published by Elsevier B.V. This is an open access article under the CC BY license (<http://creativecommons.org/licenses/by/4.0/>).

micronization) techniques without mechanical impact causing polymorph transformation [21], or reducing the stability of the pharmaceutical product [22]. By producing crystals with the desired size range further processing steps might become unnecessary; therefore, the manufacturing line can be shortened, creating a simpler and more economical production [23,24].

The IJ mixing techniques are generally used in antisolvent [14,22,23,25], reactive [14,15,26], and cooling [20,27,28] crystallizations. The IJ techniques can be grouped according to the position of nozzles as well, thus T- and Y-shaped impinging jet mixers can be separated [29,30]. The most common designs of the IJ elements are the non-submerged (or free) [23,31,32], submerged [25,33,34], and confined [13,35]. By using the free non-submerged mode, the streams have impinged in the open air then the homogeneous slurry drips directly onto a filter or – for additional crystal growth – into a vessel to approach the solubility equilibrium. In confined IJ elements, the liquid streams are mixed in a closed chamber. In submerged techniques the impinging of jets is performed under the liquid surface. The submerged mode can be coupled with ultrasonic irradiation near the mixing zone to enhance crystal size reduction and to crystallize submicron-size particles. Kügler et al. also sonicated various confined impinging jet mixers to avoid the plugging of the mixer effectively [36].

The IJ mixers can be used as an independent continuous crystallizer especially in the case of rapidly crystallizing systems, where the outlet slurry can be directly filtered. In these precipitations, further agitation is not required for appropriate yields, such as the antisolvent crystallization of ammonium perchlorate [13], or the reactive crystallization of barium sulfate [26] using a confined impinging jet reactor.

In slowly crystallizing systems the IJ mixers are applied mainly as one part of the semi-continuous or continuous crystallizer system. In these cases, the outlet of the IJ mixer is dosed into a vessel, tank, or tubular reactor to reach a higher yield before filtration. For instance, Jiang et al. [28] developed a semi-continuous crystallizer for L-asparagine monohydrate crystallization by using a DIJ as a continuous seed generator coupled with a stirred tank reactor. In the DIJ hot and cold saturated solutions collided to produce a homogeneous slurry that was fed continuously into the reactor dedicated to crystal growth. These results are the experimental validation of the simulation result previously published by Woo et al. [37]. The application of impinging jet elements in continuous crystallizers is presented only in a few reports. Liu and co-workers developed a reactive crystallization method using an IJ technique to produce sodium cefuroxime crystalline products with narrow size distribution [15,33,38]. They initiated the reaction and nucleation with an IJ mixer submerged in the solution of a continuous stirred tank reactor to ensure the sufficient and quick mixing of reactants before nucleation and also to avoid rapid spontaneous aggregation of particles. Afterward, the slurry flowed into a tubular reactor for crystal growth.

It can be stated based on the literature that the IJ technique is only used for processing pure solutions of active pharmaceutical ingredients (APIs) or fine chemicals. In addition, the impinging of liquid jets at multiple volume ratios was performed infrequently and the examples of mixing unequal liquid streams were performed only in submerged mode [15,33,38]. Furthermore, it is also underrepresented in the literature to use the combination of the IJ mixer and continuously operating MSMPR crystallizer for intensifying crystal growth. Semi-continuous configurations are utilized instead, namely the suspension leaving the IJ mixer is collected and agitated in a vessel operating in batch mode for reaching equilibrium [17,23].

The main objective of this research is to develop an alternative continuous crystallization system using an IJ mixer for the direct

Table 1

Purity, V/V Ratio, and Source of the Solvents and Solid Components in the Reaction Mixture, the Antisolvent and Solvents Used for HPLC Measurement.

	Purity	V/V %	Source
Ethyl acetate (EtOAc)		79.5	Merck Millipore
Acetic acid (AcOH)	99–100%	16.3	
Ethanol (EtOH)	≥99%	3.8	
Phosphoric acid (H ₃ PO ₄)	85 wt%	0.4	
Acetylsalicylic acid (ASA)	>99.0%	-	Sigma-Aldrich
Salicylic acid (SA)	>99.0%	-	
n-Heptane	>96.0%	-	Molar Chemicals
Acetonitrile (ACN)	>99.9%	-	Merck
Methanol (MeOH)	99.9%	-	

processing of a multi-component reaction mixture of the acetylsalicylic acid (ASA) produced in a flow synthesis [39]. Therefore, we developed a triple impinging jet mixer for the non-submerged mixing of the ASA solution and antisolvent in unequal volumetric flow rates. This in-house developed triple IJ mixer was coupled with an MSMPR crystallizer equipped with overflow tubing. The present research focuses on industrial perspectives, therefore we put more emphasis on the examination of crystal size instead of crystallization kinetics and supersaturation explanations. We aimed to examine the effect of process parameters on the product purity, the yield, the crystal size, and the CSD. Additionally, we intended to compare the developed system with our earlier results of a common overflow MSMPR crystallizer [40].

2. Experimental Materials And Methods

2.1. Materials

The composition and sources of the solvents used in the ASA reaction mixture are detailed in Table 1. For the crystallization experiments, this solution was prepared by measuring the pure components in a defined amount and stirred them until the complete dissolution of the solids. Besides ASA the reaction mixture contained various impurities, such as salicylic acid (SA) (<3%), acetylsalicylic anhydride (<1%), and others, less than a total of 5% amount in the flow synthesis mixture. As SA has the highest amount among byproducts, during the crystallization experiment the 5% SA represented the impurities in the reaction mixture. The concentration of ASA in the reaction mixture was 91.9 mg/mL (0.097 g ASA/g solvent mixture); the SA impurity concentration was 4.84 mg/mL.

2.2. Experimental methods

2.2.1. Triple Impinging Jet Mixer Setup for Mixing Unequal Flow Streams

In preliminary semi-continuous experiments, various impinging jet configurations – such as (i) dual confined IJ (angle 180°); (ii) dual free IJ (angle 180°); (iii) dual free IJ (angle 120°); (iv) triple free IJ – were tested to find the most suitable mixing technique. As (i)–(iii) configurations are known from the literature only the in-house developed triple impinging jet was described in detail. The 3D models and the picture of the triple impinging jet mixer are shown in Fig. 1.

By using a triple impinging jet mixer, three fluid streams collided. The ASA solution was dosed using a Jasco PU-980 HPLC pump. At the end of the tubing, it passed through a Supelco stainless steel capillary with 0.127 mm inner diameter (ID) to increase its linear flow velocity. The fed heptane antisolvent used in multiple quantities was divided into two liquid streams of equal volumetric flow rates. Heptane was dosed using two Knauer Azura P4.1S HPLC pumps equipped with a 10 mL stainless steel pump head. The antisolvent passed through Supelco

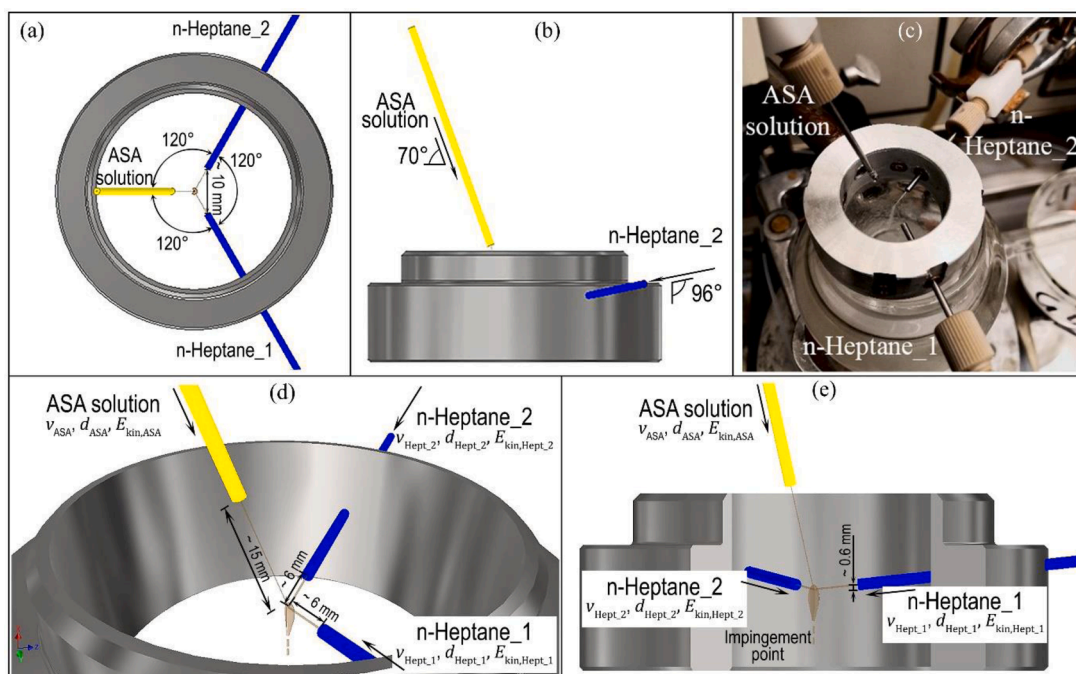


Fig. 1. 3D models and a picture of the triple impinging jet mixer from different perspectives with position descriptions (3D models were designed with Autodesk Inventor software). (a) top view; (b) side view; (c) photo of the triple impinging jet mixer; (d) diagonal view of the mixer; (e) three-quarter section of the steel circle frame.

stainless steel capillaries with a 0.254 mm ID. Capillaries with higher ID were applied for heptane feeding to decrease the difference between linear flow velocities of the streams at higher antisolvent to ASA solution ratios. The steel capillaries for heptane jets were placed in an in-house built circular steel frame with bores which was used to aid the positioning of these jets. The capillaries were angled at 120° with each other and the end of the antisolvent nozzles was ~10 mm away. To avoid the frontal collision and to facilitate the direction of impinging jets approximately 6° downward heptane jets were applied. The liquid stream of the ASA solution was introduced diagonally (approximately 70° downward) from above into the collision point of heptane streams so that the combined stream could be directed into the glass vessel more efficiently. The impingement point was approximately 6 mm far from the tip of both antisolvent capillaries and approximately 15 mm far from the tip of the

ASA capillary. The axial location of the collision was around 0.6 mm lower compared to the end of the antisolvent capillary orifice. There might be a slight difference in the positions around the given values between experiments.

Using the triple impinging jet mixer only homogeneous fluids (n-heptane antisolvent and nearly saturated ASA solution) collided. The impingement of liquid jets containing particles was not examined. The heptane jets were considered equivalent and equal, while the ASA solution stream was different regarding feeding capillary ID (stream size), feeding rate, and linear velocity. A more detailed characterization of fluid jets regarding linear velocities and kinetic energy carried by the jets is included in the Supplementary Materials.

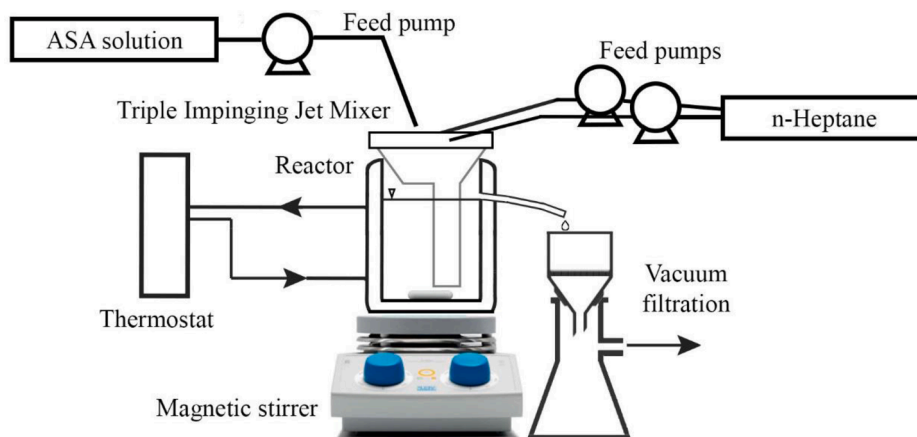


Fig. 2. Schematic image of the experimental setup.

Table 2
Set Levels of the Investigated Process Parameters.

	− (Lower)	0 (Central)	+ (Upper)
temperature [°C]	1	13	25
antisolvent to ASA solution ratio [-]	2:1	3:1	4:1
total flow rate (TFR) [mL/min] (mean RT [min])	12.5 (6.88)	15 (5.73)	17.5 (4.91)

2.2.2. Semi-Continuous Experiments with the Triple Impinging Jet Mixer

The triple impinging jet mixer was tested in a semi-continuous operation to determine the reactor size and the required mean residence time (RT) for the continuous crystallization. The flow rate of the ASA solution was set at 2.5 mL/min (3.29 m/sec linear flow velocity). Heptane flow rates were set at 5 mL/min (1.64 m/sec linear flow velocity) in each pump, so heptane was fed at a total rate of 10 mL/min. Therefore, the applied antisolvent to ASA solution ratio was 4:1 in each experiment. The suspension collected in a glass vessel was agitated continuously with a magnetic stirrer using 40 × 8 mm magnetic stirrer bars (~400 rpm) for a specified duration (0.5, 1, 2, 4, 10, and 20 min). Afterward, the suspension was vacuum filtered on either G3 or G4 glass filters. The samples were dried at room temperature to constant weight. Two series of experiments were performed at 1°C and 29°C. During the lower temperature experiments, precooled (2–3°C) heptane was mixed with ASA solution and the glass vessel was immersed in an ice bath. The order of experiments was randomized regarding post-mixing times.

The yield (y , %) was calculated by using the weight of the dried samples (m_s , g) and the nominal ASA amount (m_f , g) fed into the vessels, as follows:

$$m_f = t_f \cdot \dot{V}_s \cdot c_s \quad (1)$$

$$y = m_s / m_f \cdot 100 \quad (2)$$

, where t_f is the feeding time in min, \dot{V}_s is the volumetric flow rate of ASA solution in mL/min, and c_s is the concentration of the ASA solution in g/mL.

2.2.3. Continuous Crystallization using the Triple Impinging Jet Mixer Coupled with the MSMR Crystallizer

For the continuous crystallization experiments, the triple impinging jet mixer described in Section 2.2.1 and to ensure efficient post-mixing a jacketed glass reactor equipped with overflow tubing were used. The effective volume of the tank reactor was 86 mL. The suspension was agitated using a magnetic stirrer and a 4 cm magnetic stirring bar with 400 rpm. The jacket temperature was controlled with a monofluid thermostat (Huber Ministat 230), the temperature of the agitated suspension was measured with a Pt-100 thermometer. The schematic image of the continuous crystallization setup is illustrated in Fig. 2.

For the experiments performed at 1°C, the dosing vessel of antisolvent was cooled in an ice bath after filling with the pre-refrigerated heptane. Thus, the temperature of heptane was kept between 1–5°C throughout the feeding. The ASA solution was fed at room temperature independently of the set operation temperature to avoid undesired crystallization before the impingement. The antisolvent was dosed using a Syrris Asia syringe pump and the ASA solution was fed with a Jasco PU-980 HPLC pump. The combined liquid jet was introduced through a wide-neck funnel into the reactor. To ensure efficient mixing and to avoid the clogging of the funnel stem, half of the funnel stem was cut longitudinally. The remained half of the funnel stem served as a buffer element to prevent the immediate elimination of the fed materials through the overflow tubing. To avoid the sticking of crystals to the funnel, it was silanized.

Before the start of the continuous operation, antisolvent and ASA solution were pipetted into the reactor to prepare around 25 mL initial suspension. The amount of the pipetted fluids depended on the set

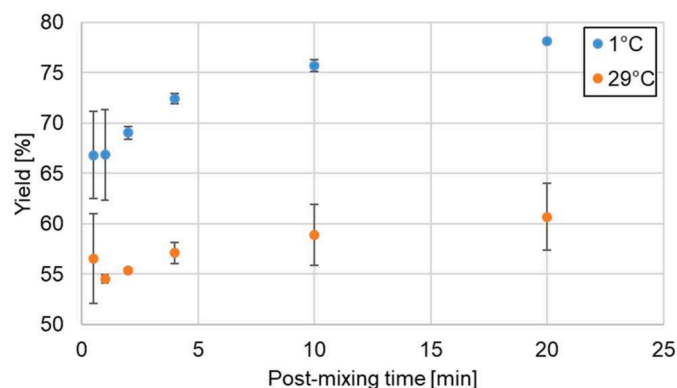


Fig. 3. Results of semi-continuous experiments, where the limits indicate \pm standard deviation values.

antisolvent to ASA solution ratio. The product was filtered directly using G3 or G4 glass filters connected to a continuously operating water jet pump. The crystals were dried at room temperature until constant weight without washing the filter cake.

Each experiment was sampled 9 times for 4–5 min depending on the mean RT. The experiments lasted for 20 RTs, as we intended to examine the system after reaching steady-state conditions. Thus, the duration of the experiments was 1.75 to 2.3 h, depending on the RTs.

To investigate the effect of crystallization parameters on product quality and quantity a 2 by 3 factorial experimental design was applied. Two parallel measurements were performed at the center point to show the reproducibility and repeatability of the results in the examined experimental region. The set levels of these parameters are detailed in Table 2. The order of the experiments was randomized. The TIBCO Statistica (version 13.5) program was used to evaluate the results of the experiments.

2.2.4. HPLC Analysis

The purity of the product was investigated with an RP-HPLC (Agilent 1200 series LC System) according to the method that was used to determine the purity of the ASA reaction mixture after the synthesis by Balogh and his co-workers [39]. From just-filtered wet samples, HPLC samples were produced by dissolving 1–5 mg of crystals in various volumes of EtOH to make a 1 mg/mL concentration solution. This solution was diluted in 1:20 ratio with a mixture of ACN:MeOH:H₃PO₄ (85%) (92:8:0.5 V/V ratio) to ensure the chemical stability of ASA [41] until the HPLC measurement. For the purity measurement, a 5 μ L sample volume was injected onto a Supelco Inertsil ODS-2 C18 column (5 μ m; 25 × 4.6 mm). Isocratic elution was performed using an eluent containing 60% ACN and 40% water–phosphoric acid mixture (200:1 ratio). The measurement lasted for 4 min; the retention time of ASA and SA were at 2.5 and 3.1 min, respectively. The impurity content of the crystalline product was determined based on the ratio of the peak areas.

2.2.5. Particle Size Distribution and Microscopic Measurements

The CSD was measured offline using a Malvern Mastersizer 2000 equipped with a Malvern Scirocco 2000 dry powder feeder. Around 100 mg of the samples were placed into the powder feeder and each measurement lasted for 6 s. The crystals were dispersed using 1 bar overpressure. The volumetric distribution values D_{v10} , D_{v50} , and D_{v90} were applied to characterize the CSD of the products. The crystal habit of the products was monitored by using a CKX53 inverse microscope equipped with an 18Mp CAM-SC180 Camera set.

Table 3

Yield and Productivity of the Experiments Carried Out with Triple Impinging Jet Mixer.

ID of experiments	T [°C]	antisolvent to ASA solution ratio [-]	TFR [mL/min]	yield [%]	productivity [g/h]
IJ_1	1	2:1	12.5	69.5 ± 5.6	16.0 ± 1.3
IJ_2	1	2:1	17.5	63.5 ± 1.9	20.4 ± 0.6
IJ_3	1	4:1	12.5	83.1 ± 4.3	11.5 ± 0.6
IJ_4	1	4:1	17.5	78.9 ± 4.4	15.2 ± 0.8
IJ_5	25	2:1	12.5	49.5 ± 3.6	11.4 ± 0.8
IJ_6	25	2:1	17.5	47.7 ± 5.0	15.3 ± 1.6
IJ_7	25	4:1	12.5	63.6 ± 2.1	8.8 ± 0.3
IJ_8	25	4:1	17.5	65.5 ± 5.0	12.6 ± 1.0
IJ_9	13	3:1	15.0	61.6 ± 5.8	12.7 ± 1.2
IJ_10	13	3:1	15.0	69.0 ± 6.0	14.3 ± 1.2

3. Results And Discussion

3.1. Semi-Continuous Crystallization with the Triple Impinging Jet Mixer

First, the widely used impinging jet mixers and an in-house developed triple impinging jet mixer were tested for mixing unequal streams. The dual confined IJ (angle 180°) was clogged shortly after the feeding was started. Using the dual free IJ (angle 180°) the collision point was shifted toward the lower velocity streams resulting in the clogging of the nozzle outlet. In the case of the dual free IJ (angle 120°) blockage did not occur, however, its drawback was the difficulty to direct the united liquid stream into the vessel, resulting in the loading of crystals on the crystallization vessel wall. In contrast, with the in-house developed triple impinging jet mixer downtime-free operation could be achieved, therefore this method proved to be the best.

Semi-continuous experiments were carried out using the triple impinging jet mixer, in order to examine the effect of the sampling duration, and thus, the post-mixing (aging) time on yield at 1°C and 29°C. The settings were repeated twice (except the experiment with 1°C and 20 min post-mixing) to receive information about reproducibility as well. The results are shown in Fig. 3.

We found that the yield could be increased by 15–23% by decreasing the temperature from room temperature to 1°C due to decreasing solubility. By extending the duration of post-mixing the yield increased, however, the speed of yield increase slowed down after 4 min at both temperatures. Therefore the equilibrium is proved to be approachable in 4–6 min. Longer aging times increased the standard deviation of the yield at room temperature, just as the short (0.5 or 1 min) aging times at both temperatures. The post-mixing time dependence of yield was slightly higher at 1°C than at 29°C. It could be explained by the activation energy of ASA cooling crystallization from ethanol [42], as activation energy is high, therefore the crystal growth is expected to be slower at lower temperatures. As a result, the MSMR crystallizer for continuous experiments was designed to operate with 4–8 min RT.

By testing the flow rates of the triple impinging jet mixer, we found that the mixing efficiency decreased by increasing the liquid flow rate difference between the collided jets. It could be caused by the splattering in the mixing region and the shift of the collision point toward the lower

Table 4The p-values, Estimates, and Confidence Intervals of the Model Coefficients ($R^2 = 0.975$).

Factors	Coeff.	p-value	-95% Conf. Limit	+95% Conf. Limit
Mean	65.16	0.0004	59.47	70.85
T [°C] (1)	-8.60	0.0229	-14.29	-2.90
AS/ASA solution [-] (2)	7.61	0.0289	1.92	13.31
TFR [mL/min] (3)	-1.27	0.4389	-6.96	4.43
1 by 2	0.37	0.8065	-5.32	6.06
1 by 3	1.31	0.4277	-4.39	7.00
2 by 3	0.68	0.6580	-5.01	6.37

velocity streams. Therefore 2:1 was chosen as the maximum ratio between fluid streams. As the antisolvent was fed with two nozzles, the maximum antisolvent to ASA solution ratio was set to 4:1.

We presume that with a few modifications this triple impinging jet technology could be further developed. With larger slopes, the collision point of the streams would be in a lower position, and thereby closer to the liquid surface in the MSMR crystallizer. We assume, that this could allow the use of higher antisolvent to ASA solution ratios and also make the introduction of the ASA solution diagonally from above into the collision point of heptane streams unnecessary. The process parameter dependence of the product quality and quantity is detailed in the following sections.

3.2. Continuous Crystallization with the Triple Impinging Jet Mixer Coupled with an MSMR Crystallizer

A series of experiments was carried out to investigate the effect of process parameters on product quality and quantity. The experiments were evaluated regarding purity, yield, productivity, and also the crystal size and CSD of the product.

3.2.1. Characterization of the Product Purity, the Process Yield, and Productivity

To determine the purification efficacy of the developed technology the last three samples of each experiment have been analyzed regarding SA content with HPLC measurement. The SA impurity content of the crystallized products was reduced from the initial 5% to $0.42 \pm 0.12\%$ on average according to the HPLC measurement. Thus, the cleaning efficiency of the developed technology was proved to be appropriate. We found that the process parameters had no significant effect on the amount and standard deviation of the impurity content in the examined experimental region.

The continuous experiments were characterized by yield and productivity as well. The yield remains constant during an experiment, therefore the average yield (y_{Av} , %) and its standard deviation ($St.dev.$, %) could be calculated using the yield of each sampling data point with the following formulas:

$$y_{Av} = \frac{\sum y_{s,x}}{n} \quad (3)$$

$$St.dev. = \sqrt{\frac{\sum (y_{s,x} - y_{Av})^2}{(n - 1)}} \quad (4)$$

where the yield of samplings ($y_{s,x}$, %) can be calculated using eqs 1 and 2; and n [-] is the number of samples. The results regarding yield and productivity are detailed in Table 3.

As the experimental region was examined according to a 2^3 full factorial design applying the rules of design of experiments (DoE),

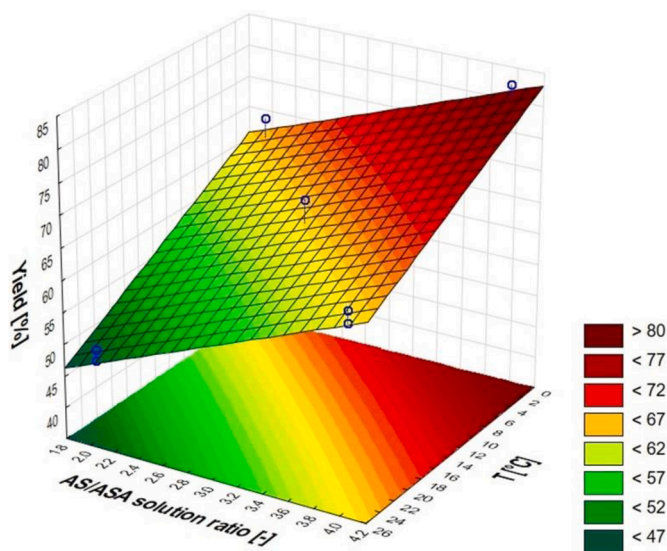


Fig. 4. Response surface showing the effect of temperature and antisolvent to ASA solution ratio on yield.

statistical analysis was carried out to investigate the process parameter dependence of yield. To investigate the curvature of the fitted model, the significance of the effects, the repeatability, and the reproducibility of crystallization in this system 2 center points (IJ_9 and IJ_10) were added to the experimental design. The selected significance level was 0.05.

Based on the result of the test, the curvature is not significant ($p > 0.05$). The investigated factors, their p -values, and their interactions with the estimates and confidence intervals of the coefficients are detailed in Table 4.

It was found that besides antisolvent to ASA solution ratio, the temperature had the most remarkable effect on product quantity. Based on the experimental data neither the TFR – and thus the RT – nor the two-way interactions were considered significant. Therefore, the yield (y , %) can be calculated with the following reduced linear model:

$$y = 51.63 - 0.72 \cdot z_T + 7.61 \cdot z_{AS/ASA} \tag{5}$$

, where z_T represents the temperature in $^{\circ}\text{C}$, and $z_{AS/ASA}$ means antisolvent to ASA solution ratio [-]. According to the diagnostic figures, the assumptions of the model are fulfilled; thus, the equation can be considered reliable. The reason for the deviation of the yield and productivity between the IJ_9 and IJ_10 experiments is the fluctuation sourced by reset of operation conditions and day-to-day variability. In such a free impingement configuration minor differences could have occurred between the implementation of the experiments. The position of each element may differ by a few mm between each experiment and might slightly be modified during experiments. Fluctuation can be sourced by the fact that the system is very sensitive to the precise placement of capillaries. Considering this the difference between IJ_9 and IJ_10 yield (appr. 7%) was acceptable.

To represent the effect of temperature and antisolvent to ASA solution ratio on yield, a Response Surface was generated using the TIBCO Statistica program (Fig. 4).

The productivity data, shown in Table 3, was primarily affected by the ASA solution flow rate that was determined by antisolvent to ASA

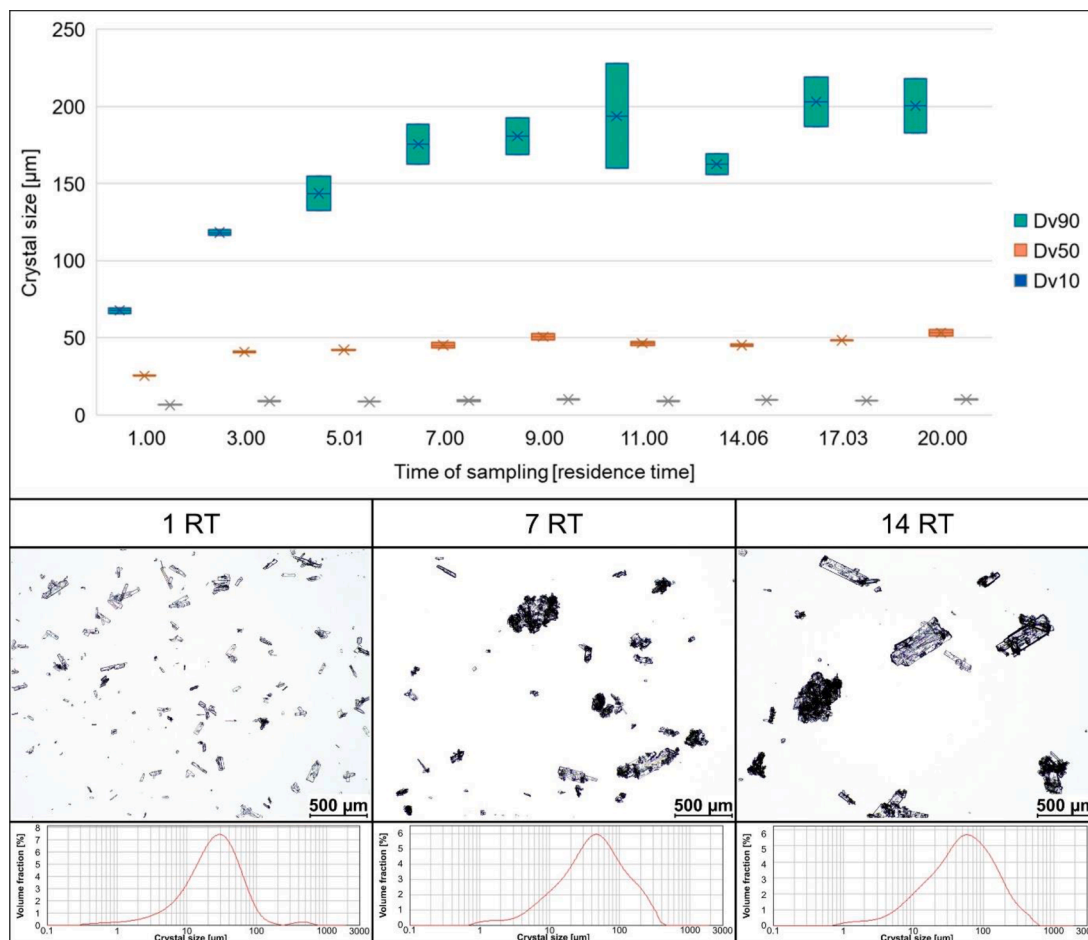


Fig. 5. Evaluation of crystal size and CSD alteration during the experiment via the example of IJ_7 (T: 25 $^{\circ}\text{C}$, AS/ASA: 4:1, TFR: 12.5 mL/min).

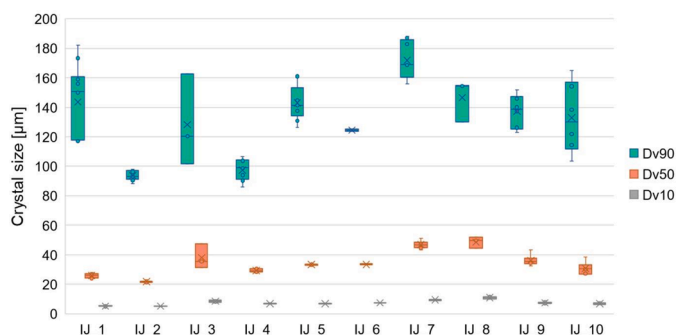


Fig. 6. Mean and standard deviation of D_{v10}, D_{v50}, and D_{v90} values in steady-state conditions.

solution ratio and TFR (and RT) together. Therefore, productivity cannot be directly connected to the examined process parameters separately. The productivity of the experiments was ranged in 8.8–20.4 g/h.

3.2.2. Characterization of Crystal Morphology

To illustrate the alteration of crystal morphology during continuous crystallization experiments using the triple IJ mixing technique, the evaluation of crystal size during the IJ_7 experiment (T: 25°C, AS/ASA: 4:1, TFR: 12.5 mL/min) is presented in Fig. 5. The CSD plots represent volume-based distributions where crystal size intervals are plotted as a function of the volume fraction (%). The volume fraction (%) of the x_i crystal size interval represents the volume percent of these crystals relative to the total crystal fraction.

As it is shown in Fig. 5, the breakage of crystals, and thus, the oscillation of crystal size during the startup period was less significant than it was in the case of a common MSMMPR crystallizer [40], or the modeling study of Szilágyi and Lakatos [43]. The individual columnar particles with narrow CSD produced after one RT were growing and the CSD was broadening during the experiment. The small particles stuck to the surface of larger crystals forming agglomerates.

As the yield was constant during the experiment, the onset of the steady-state operation was determined according to the crystal habit, size, and CSD. In the case of the IJ_7 experiment (T: 25°C, AS/ASA: 4:1, TFR: 12.5 mL/min), the steady-state was determined to be reached after the system operated for seven RTs. In the examined experimental space, the steady-state operation could be detected after the crystallization procedure has already lasted for three to seven RTs in most of the experiments regardless of the adjusted process parameters. Two exceptions were IJ_2 (T: 1°C, AS/ASA: 2:1, TFR: 17.5 mL/min) and IJ_3 (T: 1°C, AS/ASA: 4:1, TFR: 12.5 mL/min) experiments as in these cases reaching steady-state required nine and eleven RTs, respectively. After the steady-state operation was attained, the product quality and quantity were stable. The product removal was representative since the crystal habit, size, and CSD of the samplings in steady-state and the reactor content determined straight after the termination of the experiment were the same.

Fig. 6 shows the effect of the observed crystallization parameters on product size and CSD.

At lower temperatures, the produced crystals were smaller with narrower CSD, and reaching steady-state was slower. This can be caused by higher supersaturation conditions. Low temperature and longer RT (lower feed rate) can increase the standard deviation of crystal size in steady-state conditions. The similar results of the repeated experiments in the central point showed the good reproducibility of the experiments.

We analyzed the product size and CSD regarding the kinetic energy

(E_{kin}) carried by the jets as well (the calculation of jets E_{kin} are detailed in the Supplementary Materials). During the collision, the major part of the jets E_{kin} were transformed to turbulent mixing energy, therefore from the magnitude of E_{kin} we could conclude the energy of mixing. In general, we found that in the case of higher TFR (lower RT) the energy carried by the jets was higher (Table S2). At a given temperature, a smaller product with narrower CSDs was observed at higher jet E_{kin} . Considering the above, it could assume, that in the case of higher impinging energy (IJ_2 and IJ_6 with 2:1 AS/ASA ratio, 17.5 mL/min TFR; IJ_4 and IJ_8 with 4:1 AS/ASA ratio, 17.5 mL/min TFR) even more effective mixing and homogeneous nucleation occur resulting in smaller crystal size, narrower CSD, and less fluctuating particle size.

In Table 5, the microscopic pictures and CSD plots of four experiments are presented to show the effect of the process parameters on crystal habit. We found that longer RTs and lower antisolvent to ASA solution ratios enhanced the agglomeration and thereby broadened the CSD. Among shorter RTs and higher antisolvent to ASA solution ratios, a rather needle-shaped product was obtained and the number of individual crystals was higher. At lower temperatures, by reducing the RT and the antisolvent ratio the broadening of the CSD could be observed. At higher temperatures, the difference in the width of CSD is smaller by changing the TFR.

The 3D chart in Fig. 7 illustrates and summarizes the effect of the investigated process parameters on yield and average D_{v90} of the ASA products.

3.3. Comparison of Continuous Crystallization using Triple Impinging Jet Mixer to an MSMMPR Crystallization

The product of a non-submerged triple impinging mixer coupled with an overflow MSMMPR crystallizer was compared to the product of a common MSMMPR crystallizer taken from a previous publication of the authors [40]. The purity, yield, productivity, crystal habit, size, and CSD were investigated to reveal the effect of the triple impinging jet mixer on crystallization. Only those experiments were considered for the comparison in which the 4:1 antisolvent to ASA solution ratio was applied, whereas only this ratio was used at the common overflow MSMMPR crystallizer.

Besides the feeding method, the compared crystallization systems were different regarding the vessel size of the crystallizer, mixing type, and speed. The dissipation of the turbulent kinetic energy (ϵ_K , J kg⁻¹ s⁻¹) can be used to evaluate the mixing efficacy in the overflow crystallizers. If the calculated kinetic parameters are similar in the case of the compared systems then the differences could be presumably related to the use of the impinging jet mixer. The mean value of ϵ_K for stirred MSMMPR crystallizers was calculated using the following formula [44, 45]:

$$\epsilon_K = \frac{P_0 N^3 d^5}{V} \quad (6)$$


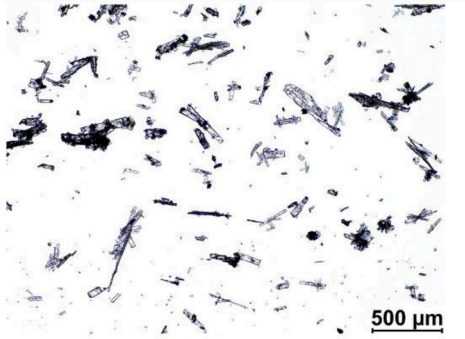
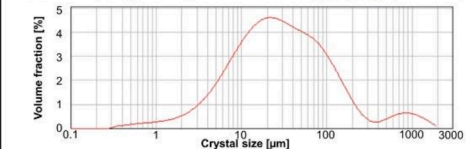
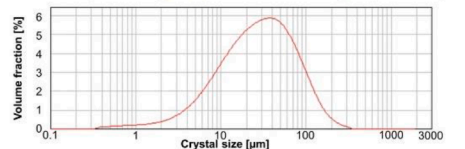
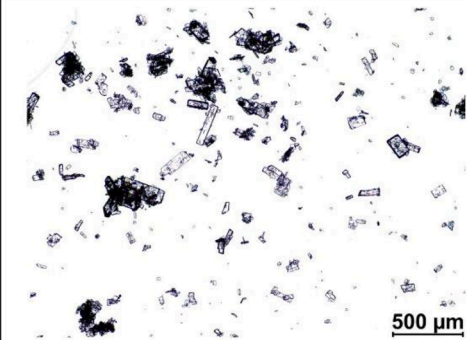
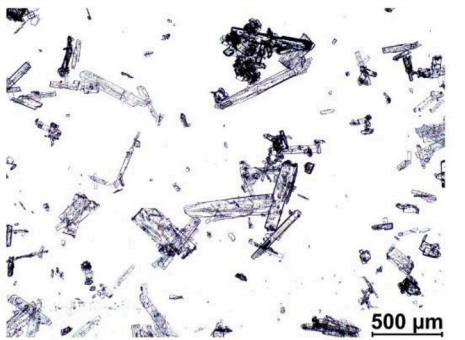
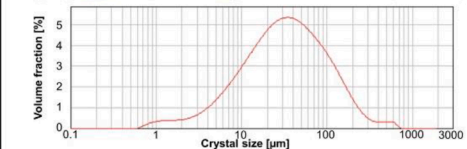
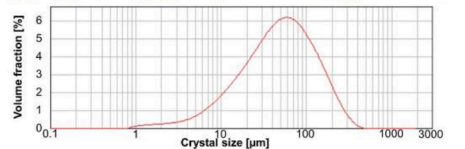
, where P_0 is the dimensionless impeller power number [-]; N is the impeller speed [round/sec]; d is the impeller diameter [m]; V is the total volume of the crystallizer [m³]. For the estimation, both the used impellers (magnetic stirrer bar and the 6-blade Rushton) were considered as bladed impellers. The system parameters used for the calculation of ϵ_K are detailed in Table 6.

The calculated ϵ_K values are very similar, therefore the crystallizations performed in different crystallization systems are proved to be comparable. Table 7 summarizes this comparison.

The SA impurity content in the triple IJ products was slightly higher compared to the products of the common MSMMPR crystallizations. In the

Table 5

Microscopic Pictures (4x), CSD Plots, and D_v10 , D_v50 , and D_v90 Values [μm] of IJ_1, IJ_4, IJ_5, and IJ_8 Experiments in Steady-State.

IJ_1 (T: 1°C; AS/ASA: 2:1; TFR: 12.5mL/min)			IJ_4 (T: 1°C; AS/ASA: 4:1; TFR: 17.5mL/min)		
					
					
D_v10	D_v50	D_v90	D_v10	D_v50	D_v90
5.2 ± 0.2	26.4 ± 2.1	159.8 ± 47.3	6.8 ± 0.2	29.2 ± 1.1	97.4 ± 6.9
IJ_5 (T: 25°C; AS/ASA: 2:1; TFR: 12.5mL/min)			IJ_8 (T: 25°C; AS/ASA: 4:1; TFR: 17.5mL/min)		
					
					
D_v10	D_v50	D_v90	D_v10	D_v50	D_v90
6.9 ± 0.1	33.3 ± 0.9	143.0 ± 12.0	10.9 ± 0.2	48.6 ± 3.7	146.5 ± 14.1

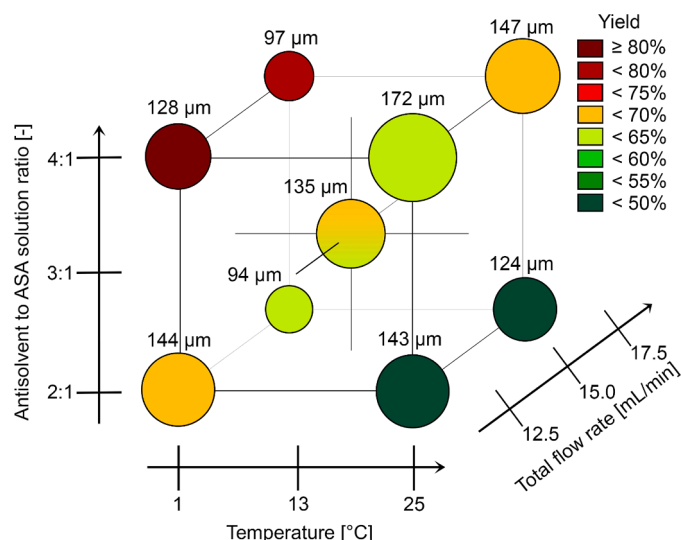


Fig. 7. 3D chart to represent the average $D_{v,90}$ values and yield of the experiments as a function of temperature, antisolvent to ASA solution ratio, and TFR.

Table 6

Dissipation of Turbulent Kinetic Energy Calculation in the Case of the Compared MSMPR Crystallization Systems.

System	Overflow MSMPR Crystallizer (86 ml)	Overflow MSMPR Crystallizer (235 mL)
Impeller type	magnetic stirrer bar	6-blade Rushton
P_0 [-]	5	5
N [round/sec]	6.67	11.67
d [m]	$4.00 \cdot 10^{-2}$	$3.50 \cdot 10^{-2}$
V [m ³]	$8.60 \cdot 10^{-5}$	$2.35 \cdot 10^{-4}$
ϵ_K [m ² s ⁻³]	1.764	1.775

developed continuous technology using a triple impinging jet mixer, the average crystal size was lower resulting in a larger crystal surface. In absence of washing, the mother liquor remained on the crystal surface could be higher slightly increasing the impurity content of the product.

It can be stated by comparing technologies that the system including a triple impinging jet mixer can be operated with similar productivity as the 235 mL one-stage overflow MSMPR crystallizer. However, the product quality was remarkably different: with the triple impinging jet mixer, the crystal size varied in the range of 8 to 180 μm , while the size of the product fell in the range of 80 to 600 μm in a 235 mL MSMPR crystallizer. The fluctuations in $D_{v,10}$, $D_{v,50}$, and $D_{v,90}$ values of the samples collected at steady-state conditions are more significant using the larger MSMPR crystallizer that was not equipped with an impinging jet mixer.

By using a triple impinging jet mixer, the temperature has a smaller effect on the shape of CSD plots, as the rapid mixing before nucleation ensures the homogeneous nucleation and thereby the narrower CSD. By applying the 235 mL MSMPR crystallizer, the efficacy of mixing is lower, therefore the nucleation is less homogeneous especially at lower temperatures, where the supersaturation is higher. As a consequence, the product of this technology has a broader CSD that can be polydisperse or unimodal depending on the operating temperature.

The impinging mixing technique can influence each of the crystallization mechanisms through supersaturation (model equations

describing the crystallization mechanisms are summarized in Table S3). With the triple impinging jet mixer more homogeneous supersaturation and temperature can be reached compared to regular feeding methods. Homogeneous supersaturation initiated by effective mixing resulting in lower fluctuation in crystal size and habit and a more reproducible crystallization process compared to regular feeding methods.

When the kinetic energy of the jets was lower, slightly higher fluctuation in crystal size could be experienced due to less effective mixing. Using a triple impinging jet mixer, the temperature dependence of crystal size and crystal habit, which was experienced in common MSMPR crystallizers has vanished. According to the equations, it was also expected that reaching the steady-state operation in the developed system with a triple impinging jet mixer is faster compared to the common MSMPR crystallizer. This is also supported by experimental results.

4. Conclusion

The results published regarding impinging jet mixers, used for continuous or semi-continuous crystallization, applied without exception dual mixers with two jets. In these studies, pure solutions of the model active ingredient were processed, therefore, the purification efficacy could not be examined. In contrast, in the present study, we aimed to develop a continuous crystallization technology for the purification and separation of a multicomponent reaction mixture using an in-house developed impinging jet mixer. Efficient mixing was achieved with the designed triple impinging jet mixing technique even when the ratio of the liquid streams was unequal. The mixer was combined with an overflow MSMPR crystallizer to provide an appropriate time for nucleation and crystal growth before filtration. The overflow tubing allowed a pump-free continuous withdrawal of the slurry without the mechanical degradation of the crystalline product.

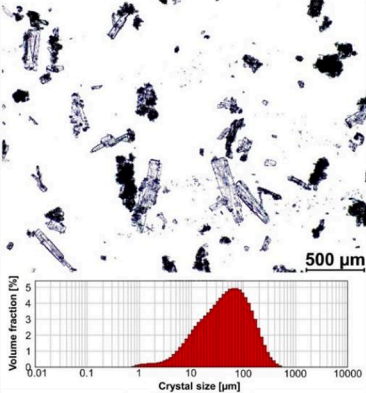
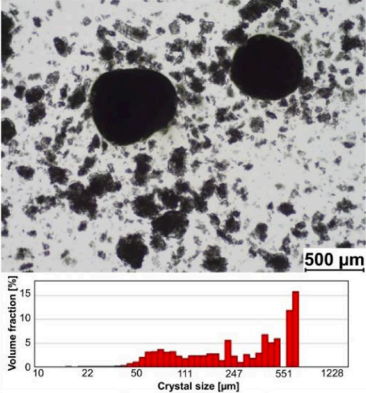
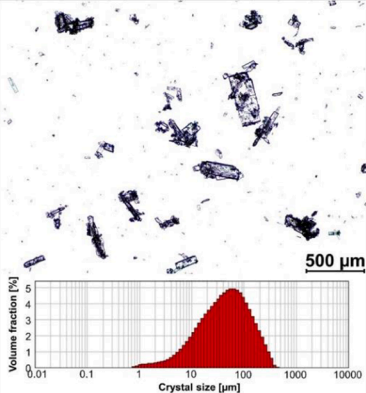
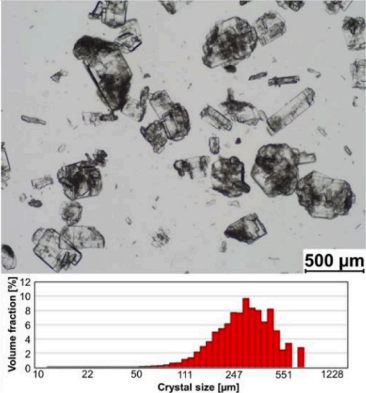
The dependence of the purity, yield, crystal size, habit, and CSD on the process parameters – such as temperature, RT, and antisolvent to ASA solution ratio – was investigated. It was found that neither of the examined parameters affected the product purity that was slightly lower than in the case of the previously published MSMPR crystallizer. The significant impact of the antisolvent to ASA solution ratio and the temperature on yield was observed, while the TFR (and thus RT) did not alter the yield considerably. The yield can be increased by 15–20% by decreasing the temperature and by around 15% by increasing the antisolvent to ASA solution ratio from 2:1 to 4:1. Under the most favorable operating conditions – at low temperature and high antisolvent to ASA solution ratio – the average yield of 83.1% was achieved.

The product – that contained columnar crystals – was characterized by unimodal CSD ranging in size from 8 to 180 μm . The CSD was most affected by the temperature, RT, and the energy carried by the jets. Increasing operation temperature caused larger product in size, while the decrease of RT – and thus, an increase of the TFR and the energy carried by the jets – resulted in narrower CSD and smaller particle size fluctuations at steady state conditions due to more effective mixing.

By comparing the results of the crystallization coupled with impinging jet technology with the product of the 235 mL overflow MSMPR crystallizer, it was found that the triple impinging jet technique can be more efficient when a product with a small crystal size and narrow unimodal CSD is required. The concept of the developed technology is proved to be an effective alternative to the most popular crystallization technologies (MSMPR and PF crystallizer). It can be used not only for the direct processing of a flow reaction mixture but also for the modification of product quality preserving the same productivity.

Table 7

Comparison of the Triple Impinging Jet Mixer Coupled with an Overflow MSMPR Crystallizer to a Common Overflow MSMPR Crystallizer.

parameters	Triple Impinging Jet Mixer Coupled with an Overflow MSMPR Crystallizer (86 mL)	Overflow MSMPR Crystallizer (235 mL)				
Residence time	4.91 – 6.88 min	11.75 – 47.00 min				
Purity	0.42 ± 0.12%	0.30 ± 0.16%				
Yield	63.6 – 83.1%	57.6 – 78.6%				
Productivity	8.8 – 15.2 g/h	3.2 – 17.3 g/h				
Microscopic pictures (4x), CSD, and D _v 10, D _v 50, D _v 90 values in μm	1 °C					
						
	D _v 10	D _v 50	D _v 90	D _v 10	D _v 50	D _v 90
	8 ± 1	38 ± 8	128 ± 31	83 ± 19	326 ± 48	577 ± 95
	25 °C					
						
	D _v 10	D _v 50	D _v 90	D _v 10	D _v 50	D _v 90
	9 ± 0	47 ± 3	172 ± 13	165 ± 5	311 ± 14	531 ± 51

CrediT authorship contribution statement

Kornélia Tacsí: Conceptualization, Methodology, Investigation, Validation, Visualization, Writing - Original Draft, Writing - Review & Editing. Ádám Joó: Investigation. Éva Pusztai: Formal analysis, Writing - Review & Editing. András Domokos: Writing - Review & Editing. Zsombor K. Nagy: Conceptualization. György Marosi: Conceptualization, Supervision, Writing - Review & Editing. Hajnalka Pataki: Conceptualization, Methodology, Supervision, Writing - Review & Editing.

Declaration of Competing Interest

The authors declare that they have no known competing financial interests or personal relationships that could have appeared to influence the work reported in this paper.

Acknowledgement

This work was performed in the frame of the FIEK_16-1-2016-0007 project, implemented with the support provided by the National Research, Development, and Innovation Fund of Hungary, financed under the FIEK_16 funding scheme. Hajnalka Pataki is thankful for the János Bolyai Research Scholarship of the Hungarian Academy of Sciences. This work was financially supported by the National Research, Development and Innovation Office of Hungary (OTKA PD-121143, KH-129584, FK-132133). The research was also supported by the ÚNKP-20-3-I-BME-310 and the ÚNKP-20-5-BME-307 New National Excellence Program of the Ministry for Innovation and Technology from the source of the National Research, Development, and Innovation Fund. We would like to thank Botond Szilágyi for his help in the revision procedure.

Supplementary materials

Supplementary material associated with this article can be found, in the online version, at doi:10.1016/j.cep.2021.108446.

References

- [1] M. Kakran, N.G. Sahoo, L. Li, Z. Judeh, Particle size reduction of poorly water soluble artemisinin via antisolvent precipitation with a syringe pump, *Powder Technol.* 237 (2013) 468–476, <https://doi.org/10.1016/j.powtec.2012.12.029>.
- [2] M.A. Kurup, R. Raj, Antisolvent Crystallization: a novel approach to bioavailability enhancement, *Eur. J. Biomed. Pharm. Sci.* 3 (2016) 230–234.
- [3] K. Krupa, M.I. Nunes, R.J. Santos, J.R. Bourne, Characterization of micromixing in T-jet mixers, *Chem. Eng. Sci.* 111 (2014) 48–55, <https://doi.org/10.1016/j.ces.2014.02.018>.
- [4] T. Koiranen, M. Woldemariam, A. Salminen, Reactor performance and design concept in additively manufactured milli-scale reactors, *J. Chem. Eng. Process Technol.* 08 (2017) 363, <https://doi.org/10.4172/2157-7048.1000363>.
- [5] B. Wu, J. Li, C. Li, J. He, P. Luo, Antisolvent crystallization intensified by a jet crystallizer and a method for investigating crystallization kinetics, *Chem. Eng. Sci.* 211 (2020), 115259, <https://doi.org/10.1016/j.ces.2019.115259>.
- [6] B. Wu, Y. Fang, C. Zhao, Y. Wang, P. Luo, Experimental study and numerical simulation of barium sulfate precipitation process in a continuous multi-orifice-impinging transverse jet reactor, *Powder Technol.* 321 (2017) 180–189, <https://doi.org/10.1016/j.powtec.2017.08.042>.
- [7] P. Luo, Y. Fang, B. Wu, H. Wu, Turbulent characteristics and design of transverse jet mixers with multiple orifices, *Ind. Eng. Chem. Res.* 55 (2016) 8858–8868, <https://doi.org/10.1021/acs.iecr.6b01778>.
- [8] M. Kreimer, M. Zettl, I. Aigner, T. Mannschott, P. Van Der Wel, J.G. Khinast, M. Krumme, Performance characterization of static mixers in precipitating environments, *Org. Process Res. Dev.* 23 (2019) 1308–1320, <https://doi.org/10.1021/acs.oprd.8b00267>.
- [9] Y. Dong, W.K. Ng, J. Hu, S. Shen, R.B.H. Tan, A continuous and highly effective static mixing process for antisolvent precipitation of nanoparticles of poorly water-soluble drugs, *Int. J. Pharm.* 386 (2010) 256–261, <https://doi.org/10.1016/j.ijpharm.2009.11.007>.
- [10] M. Jiang, C.D. Papageorgiou, J. Waetzig, A. Hardy, M. Langston, R.D. Braatz, Indirect ultrasonication in continuous slug-flow crystallization, *Cryst. Growth Des.* 15 (2015) 2486–2492, <https://doi.org/10.1021/acs.cgd.5b00263>.
- [11] O.V. Proskurina, R.S. Abiev, D.P. Danilovich, V.V. Panchuk, V.G. Semenov, V. N. Nevedomsky, V.V. Gusarov, Formation of nanocrystalline BiFeO₃ during heat treatment of hydroxides co-precipitated in an impinging-jets microreactor, *Chem. Eng. Process. Process Intensif.* 143 (2019), 107598, <https://doi.org/10.1016/j.cep.2019.107598>.
- [12] S. Pal, K. Madane, A.A. Kulkarni, Antisolvent based precipitation: batch, capillary flow reactor and impinging jet reactor, *Chem. Eng. J.* 369 (2019) 1161–1171, <https://doi.org/10.1016/j.cej.2019.03.107>.
- [13] A.J. Mahajan, D.J. Kirwan, Micromixing effects in a two-impinging-jets precipitator, *AIChE J.* 42 (1996) 1801–1814, <https://doi.org/10.1002/aic.690420702>.
- [14] W.J. Liu, C.Y. Ma, J.J. Liu, Y. Zhang, X.Z. Wang, Analytical technology aided optimization and scale-up of impinging jet mixer for reactive crystallization process, *AIChE J.* (2015) 503–517, <https://doi.org/10.1002/aic>.
- [15] J. Zhang, Y. Liu, Y. Luo, The turbulent behavior of novel free triple-impinging jets with large jet spacing by means of particle image velocimetry, *Chin. J. Chem. Eng.* 24 (2016) 757–766, <https://doi.org/10.1016/j.cjche.2016.04.022>.
- [16] T. Tari, P. Szabó-Révész, Z. Aigner, Comparative study of different crystallization methods in the case of cילותazol crystal, *Crystals* 9 (2019) 295.
- [17] F. Kesisoglou, S. Panmai, Y. Wu, Nanosizing - Oral formulation development and biopharmaceutical evaluation, *Adv. Drug Deliv. Rev.* 59 (2007) 631–644, <https://doi.org/10.1016/j.addr.2007.05.003>.
- [18] M. Jiang, R.D. Braatz, Designs of continuous-flow pharmaceutical crystallizers: developments and practice, *CrystEngComm* 21 (2019) 3534–3551, <https://doi.org/10.1039/c8ce00042e>.
- [19] M. Jiang, Y.E.D. Li, H.H. Tung, R.D. Braatz, Effect of jet velocity on crystal size distribution from antisolvent and cooling crystallizations in a dual impinging jet mixer, *Chem. Eng. Process. Process Intensif.* 97 (2015) 242–247, <https://doi.org/10.1016/j.cep.2015.09.005>.
- [20] B. Shekunov, P. York, Crystallisation processes in pharmaceutical technology and drug delivery, *J. Cryst. Growth.* 211 (2000) 122–136.
- [21] J.M. Midler, E.L. Paul, E.F. Whittington, M. Futran, P.D. Liu, J. Hsu, S.H. Pan, Crystallization Method to Improve Crystal Structure and Size, 1994, 5314506A.
- [22] T. Tari, Z. Fekete, P. Szabó-Révész, Z. Aigner, Reduction of glycine particle size by impinging jet crystallization, *Int. J. Pharm.* 478 (2015) 96–102, <https://doi.org/10.1016/j.ijpharm.2014.11.021>.
- [23] X.Y. Woo, R.B. Tan, R.D. Braatz, Modeling and computational fluid dynamics-population balance equation-micromixing simulation of impinging jet crystallizers, *Cryst. Growth Des.* 9 (2009) 156–164, <https://doi.org/10.1021/cg800095z>.
- [24] M.D. Lindrud, S. Kim, C. Wei, Sonic Impinging Jet Crystallization Apparatus and Process, 2001.
- [25] D.L. Marchisio, L. Rivautella, A.A. Barresi, Design and scale-up of chemical reactors for nanoparticle precipitation, *AIChE J.* 52 (2006) 1877–1887, <https://doi.org/10.1002/aic>.
- [26] M. Jiang, C. Gu, R.D. Braatz, Understanding temperature-induced primary nucleation in dual impinging jet mixers, *Chem. Eng. Process. Process Intensif.* 97 (2015) 187–194, <https://doi.org/10.1016/j.cep.2015.06.013>.
- [27] M. Jiang, M.H. Wong, Z. Zhu, J. Zhang, L. Zhou, K. Wang, A.N. Ford Versypt, T. Si, L.M. Hasenberg, Y.E. Li, R.D. Braatz, Towards achieving a flat-top crystal size distribution by continuous seeding and controlled growth, *Chem. Eng. Sci.* 77 (2012) 2–9, <https://doi.org/10.1016/j.ces.2011.12.033>.
- [28] L. Metzger, M. Kind, On the transient flow characteristics in Confined Impinging Jet Mixers - CFD simulation and experimental validation, *Chem. Eng. Sci.* 133 (2015) 91–105, <https://doi.org/10.1016/j.ces.2014.12.056>.
- [29] J. Gradl, H.C. Schwarzer, F. Schwertfirm, M. Manhart, W. Peukert, Precipitation of nanoparticles in a T-mixer: coupling the particle population dynamics with hydrodynamics through direct numerical simulation, *Chem. Eng. Process. Process Intensif.* 45 (2006) 908–916, <https://doi.org/10.1016/j.cep.2005.11.012>.
- [30] T. Tari, R. Ambrus, G. Szakonyi, D. Madarász, J. Ulrich, Optimizing the crystal habit of Glycine by using an additive for impinging jet crystallization, *Chem. Eng. Technol.* (2017) 1323–1331, <https://doi.org/10.1002/ceat.201600634>.
- [31] B. Rimez, J. Conté, E. Lecomte-Norrand, P. Cognet, C. Gourdon, B. Scheid, Continuous-flow tubular crystallization to discriminate between two competing Crystal Polymorphs. 2. Antisolvent Crystallization, *Cryst. Growth Des.* 18 (2018) 6440–6447, <https://doi.org/10.1021/acs.cgd.8b00930>.
- [32] W.J. Liu, C.Y. Ma, X.Z. Wang, Continuous Reactive Crystallization of Pharmaceuticals Using Impinging Jet Mixers, *Am. Inst. Chem. Eng. J.* 63 (2017) 967–974, <https://doi.org/10.1002/aic>.
- [33] D.J. Am Ende, T.C. Crawford, N.P. Weston, *React. Crystal. Method Improve Particle Size* (2003). US 6,558,435 B2.
- [34] D.L. Marchisio, L. Rivautella, A.A. Barresi, I. Chimica, Design and Scale-Up of Chemical Reactors for Nanoparticle Precipitation, *AIChE J.* 52 (2006) 1877–1887, <https://doi.org/10.1002/aic>.
- [35] R.T. Kügler, M. Kind, Experimental study about plugging in confined impinging jet mixers during the precipitation of strontium sulfate, *Chem. Eng. Process. Process Intensif.* 101 (2016) 25–32, <https://doi.org/10.1016/j.cep.2015.12.007>.
- [36] X.Y. Woo, R.B.H. Tan, R.D. Braatz, Precise tailoring of the crystal size distribution by controlled growth and continuous seeding from impinging jet crystallizers, *Cryst. Eng. Comm.* 13 (2011) 2006–2014, <https://doi.org/10.1039/c0ce00637h>.
- [37] W.J. Liu, C.Y. Ma, X.Z. Wang, Novel impinging jet and continuous crystallizer design for rapid reactive crystallization of pharmaceuticals, *Procedia Eng.* 102 (2015) 499–507, <https://doi.org/10.1016/j.proeng.2015.01.199>.
- [38] A. Balogh, A. Domokos, B. Farkas, A. Farkas, Z. Rapi, D. Kiss, Z. Nyiri, Z. Eke, G. Szarka, R. Örkényi, B. Mátravölgyi, F. Faigl, G. Marosi, Z.K. Nagy, Continuous end-to-end production of solid drug dosage forms: coupling flow synthesis and formulation by electrospinning, *Chem. Eng. J.* 350 (2018) 290–299, <https://doi.org/10.1016/j.ces.2018.05.188>.
- [39] K. Tacsí, H. Pataki, A. Domokos, B. Nagy, I. Csontos, I. Markovits, F. Farkas, Z. K. Nagy, G. Marosi, Direct processing of a flow reaction mixture using continuous mixed suspension mixed product removal Crystallizer, *Cryst. Growth Des.* (2020), <https://doi.org/10.1021/acs.cgd.0c00252>.
- [40] J. Fogel, P. Epstein, P. Chen, Simultaneous high-performance liquid chromatography assay of acetylsalicylic acid and salicylic acid in film-coated aspirin tablets, *J. Chromatogr. A.* 317 (1984) 507–511.
- [41] J. Glasby, K. Ridgway, The crystallization of aspirin from ethanol, *J. Pharm. Pharmacol.* 20 (1968) 94S–103S, <https://doi.org/10.1111/j.2042-7158.1968.tb09868.x>.
- [42] B. Szilágyi, B.G. Lakatos, Model-based analysis of stirred cooling crystallizer of high aspect ratio crystals with linear and nonlinear breakage, *Comput. Chem. Eng.* 98 (2017) 180–196, <https://doi.org/10.1016/j.compchemeng.2016.11.028>.
- [43] A. Imran, E. Wolf, H.J.M. Kramer, P.J. Jansens, Contribution of crystal-impeller and crystal-crystal collisions to secondary nucleation, *Eur. Congr. Chem. Eng.* (2007) 16–20.
- [44] B. Nagy, B. Szilágyi, A. Domokos, K. Tacsí, H. Pataki, G. Marosi, Z. Kristóf Nagy, Z. K. Nagy, Modeling of pharmaceutical filtration and continuous integrated crystallization-filtration processes, *Chem. Eng. J.* (2020), 127566, <https://doi.org/10.1016/j.ces.2020.127566>.